Optimal Decompression of Divers

Procedures for Constraining Predicted Bubble Growth

CHRISTIAN R. GUTVIK, TOR A. JOHANSEN, and ALF O. BRUBAKK

The human body is not adapted for living underwater, but mankind's abilities to invent, create, and use technical equipment allows underwater breathing. The activity of diving started as free diving, where the diver's lung capacity was the limiting factor. In the 18th century the invention of the diving suit made it possible to supply divers with air from the surface. Although economically profitable, this invention was disastrous for divers, who sometimes suffered from extreme pain, permanent paralysis, and occasionally death. These symptoms were initially named caisson disease [1] but are now classified as decompression sickness (DCS).

Diving (see Figure 1) involves breathing either pressurized air or a gas mixture consisting of oxygen plus one or more inert gas, typically nitrogen or helium. Oxygen is transported in blood 99% bound to hemoglobin and is metabolized in cellular processes. However, the pressurized inert gas reaches equilibrium with its environment by rapid diffusion across the alveoli membrane in the lungs to the arterial side of the circulatory system. This gas is transported in the bloodstream to body tissues, where it accumulates over time [2].

During ascent to the surface, the inert gas may come out of solution and form gas bubbles, which cause DCS. This process is similar to what occurs when the cork is popped from a bottle of champagne, where bubbles instantly form when the pressure drops. To prevent bubble growth, decompression procedures are performed to allow divers to ascend safely from depth. By making controlled stops during the ascent to the surface, time is allowed for the blood circulation to wash out the excess inert gas through the lungs, thus preventing a pressure drop sufficient to cause significant bubble growth. These procedures are calculated by a decompression algorithm, which is implemented either as a precalculated table, dive-planning software, or a real-time dive-computer algorithm. A decompression procedure is used by the diver if the combination of bottom depth and time exceeds a no-decompression-limit (NDL).

The first decompression model, created in 1908 [3], uses multiple, parallel tissue compartments with different time constants, where first-order linear equations describe inert-gas partial pressures. A drop in ambient pressure results in supersaturation, which is defined as the ratio between the compartment-gas partial pressure and the ambient pressure. The decompression procedures are calculated by setting a threshold for acceptable supersaturation at each instant of time. This approach yields a simple, analytical solution for how long the diver must remain at each decompression stage. Despite more than 100 years of decompression research, this model remains the foundation of most current algorithms and tables.

Advances in electronics and computer technology over the last few decades have given birth to dive computers. A diver carries these small electronic devices during the dive and continually measures depth and time spent under water. The decompression algorithms used to calculate

NILS AUKAN

FIGURE 1 Diver in water. Decompression along an anchor line is cold, boring, time wasting, and generally undesirable. The objective of the work presented in this article is to minimize the time spent decompressing.

Digital Object Identifier 10.1109/MCS.2010.939141
Date of publication: 13 January 2011

decompression tables for predive planning are adapted for dive computer implementation. The methodology for calculating decompression procedures is simple enough for fixed-point arithmetic in low-power, embedded processors.

Since these algorithms are based on a supersaturation threshold, the underlying models use arbitrary stress predictors, and hence the model outcome itself is not of interest. Furthermore, since the algorithms are benchmarked only on their success in preventing DCS, they do not offer a quantitative risk assessment. The model parameters are empirically tuned to achieve an acceptable risk of the binary outcome, namely DCS or no DCS. These statements are also true for modern decompression algorithms, such as the varying permeability model (VPM) [4] and the reduced-gradient bubble model (RGBM) [5].

Although more complex gas-separation models are available [6]–[8], their practical use is limited by model outputs, which are not measurable stress predictors. The bubble dynamics model developed in [9] uses the integral of bubble volume as a risk function. This model is validated using logistic regression analysis with an extensive database of DCS incidence. However, bubble volume is not measurable, resulting in model mechanics that are weakly validated by data fitting. A common property of these dynamic bubble-formation models is that the calculation of decompression procedures is difficult. Since analytical solutions are not available for these models, iterative, numerical methods that simulate the predicted model output are needed. However, no such methodology is available, and thus these models are not close to being operational for dive-computer implementation.

The nonlinear, dynamic, dual-phase bubble model Copernicus [10] uses venous gas emboli (VGE) as the decompression stress predictor. This model is validated against measured data using ultrasound imaging and Doppler ultrasonic methods to detect vascular gas bubbles [11] and is further refined to account for individual differences and in-dive workload estimates [12]. VGE is currently the only known quantitative measure of decompression stress, and as shown in [13] and [14], VGE is a sensitive and reliable risk predictor for DCS, where an absence of large numbers of VGE is a strong predictor of symptom-free dives.

For all diving activity, including commercial, recreational, technical, and military, the time spent on decompression is undesirable. A decompression procedure can thus be considered to be a compromise between safety and time efficiency. The approach described in this article uses the Copernicus model to repeatedly solve, using numerical methods, the optimal control problem to minimize total decompression time. The constraint is a critical limit to the post-dive bubble volume as determined by model predictive control (MPC) [15]. MPC was initially developed for the chemical process industry and further adopted by the biomedical sciences [16], [17]. Optimal control theory is used in [18] to analyze ascent rates from a dive under a supersaturation model.

By using a model with a measurable stress predictor as the foundation, the predictor can provide additional useful information to the diver. The consequence of not following the advised profile exactly can be evaluated, for example, by observing the extent of bubble-growth constraint violation after an emergency ascent. Since the Copernicus model is individually adaptive and compensates for in-dive workload, the calculated decompression profiles take these factors into account. The purpose of this article is thus to present the diving decompression problem as an optimal control application. Additional technical issues are studied in [19] and [20].

DYNAMIC MODEL

Copernicus is a dual-phase dynamic model of vascular gas-bubble formation in divers [10]. Using imaging and Doppler methods, the model is fit to ultrasonic measurements of VGE following human dives [11]. The optimal control problem is designed to set a threshold for tolerated VGE peak, which is considered to be associated with a sufficiently low risk of DCS. The VGE peak can be numerically integrated using the dynamic model

$$\dot{x} = f(x, u, w), \tag{1}$$

$$y = h_m(x, w), \tag{2}$$

where

$$f(x,u,w) = \begin{bmatrix} \dfrac{D\alpha_b}{h}\left(P_{t,1} - P_{\text{amb}} - \dfrac{2\gamma}{r_1} + P_{\text{meta}} + \dfrac{c_s}{r_1^3}\right) - \dfrac{r_1}{3}u \\ \hline P_{\text{amb}} + \dfrac{4\gamma}{3r_1} - P_{\text{meta}} \\ \varepsilon_{\tau,1}\omega_1 \dfrac{\alpha_b}{\alpha_{t,1}}\left(f_{N_2}P_{\text{amb}} - P_{t,1}\right) \\ \dfrac{D\alpha_b}{h}\left(P_{t,2} - P_{\text{amb}} - \dfrac{2\gamma}{r_2} + P_{\text{meta}} + \dfrac{c_s}{r_2^3}\right) - \dfrac{r_2}{3}u \\ \hline P_{\text{amb}} + \dfrac{4\gamma}{3r_2} - P_{\text{meta}} \\ \varepsilon_{\tau,2}\omega_2 \dfrac{\alpha_b}{\alpha_{t,2}}\left(f_{N_2}P_{\text{amb}} - P_{t,2}\right) \\ u \end{bmatrix}, \tag{4}$$

$$h_m(x,w) = \frac{4\pi}{3}\sum_{i=1}^{2} K_{m,i} r_i^3 V_i \omega_i - V_0, \tag{5}$$

$$x = \begin{bmatrix} r_1 & p_{t,1} & r_2 & p_{t,2} & P_{\text{amb}} \end{bmatrix}^T, \tag{6}$$

$$u = \dot{P}_{\text{amb}}, \tag{7}$$

$$w = \begin{bmatrix} f_{N_2} & \omega_1 & \omega_2 \end{bmatrix}^T. \tag{8}$$

TABLE 1 Overview of the parameters of the Copernicus model. The estimated parameters are a result of the numerical parameter estimation in [11], whereas the model coefficients are given in the cited literature. Values for the diffusivity D/h and the dead volume for detection V_0 are not available. The solubility in muscle tissues $\alpha_{t,1}$ is chosen based on a fraction of water and fat content. The state space, input, and noise parameters describing the vectors x, u, and w are defined in (7) and(8).

Par.	Description	Unit	Value	Refs.
Estimated parameters				
$\varepsilon_{\tau,1}$	Time constant correction muscles	—	0.189	[11]
$\varepsilon_{\tau,2}$	Time constant correction fat	—	0.900	[11]
γ	Surface tension	10^{-3} N/m	39.0	[11]
$K_{m,1}$	Measurement gain muscle	—	1.079×10^{-5}	[11]
$K_{m,2}$	Measurement gain fat	—	0.6886×10^{-4}	[11]
Model coefficients				
r_0	Initial bubble radius	μm	1	[7]
$\frac{D}{h}$	Diffusivity	μm/min	300	—
α_b	Blood solubility	1/kPa	1.58×10^{-4}	[35]
$\alpha_{t,1}$	Tissue solubility in muscles	1/kPa	2.78×10^{-4}	[35]
$\alpha_{t,2}$	Tissue solubility in fat	1/kPa	6.4×10^{-4}	[35]
P_{meta}	Partial pressure of metabolic gases	1/kPa	17.73	[8]
V_1	Tissue volume muscles	dm^3	28.4	[36]
V_2	Tissue volume fat	dm^3	11.7	[36]
V_0	Dead volume for detection	# bubbles/ cm^2/min	0.005	—
State space, input, and noise				
r_i	Bubble radius	μm	—	—
$p_{t,i}$	Tissue partial pressure	kPa	—	—
P_{amb}	Ambient pressure	kPa	—	—
f_{N_2}	Fraction of nitrogen in breathing gas	—	—	—
ω_i	Blood perfusion	1/min	—	—

The input P_{amb}, which is the measured depth change response of the diver, is the parameter used to recommend control actions in terms of an ascent profile to the diver through the user interface of the dive computer. The vector w contains parameters that can be considered as known disturbances to the model. The measurement function (4) is a scalar output expressing the number of bubbles detected in the venous pool over time using ultrasonic image scanning [21]. The parameter c_s is given by [10]

$$c_s = r_0^3\left(P_{\text{amb,surf}}\,(1 - f_{N_2,\text{air}}) + \frac{2\gamma}{r_0} - P_{\text{meta}}\right), \tag{9}$$

where $P_{\text{amb,surf}}$ is the ambient pressure at surface, and $f_{N_2,\text{air}} = 0.78$ is the fraction of nitrogen in air. All other parameters of the model are given in Table 1. The model has two distinct purposes in a dive computer, namely, to be used as a model-based state estimator to find the initializing parameter vector for the optimal control problem and to predict the future response for the optimal control algorithm. Thus, there are some slight differences in how the model is interpreted.

State Estimator

At each time during the dive, the state of the diver is updated. Model (2)–(8) is implemented as a state observer with $\Delta T = 4$ s sampling time using Euler integration, that is,

$$x_{k+1} = x_k + \Delta T f(x_k, u_k, w_k). \tag{10}$$

However, the state vector is not observable through available measurements in real time since only the input u and noise w are measured, and thus the observer must be run open loop. Thus, the reliability of the procedure is entirely dependent on the accuracy and robustness of the model itself. The input u is measured by a pressure sensor and is a result of the diver's own diving objectives and interpretation of the feedback from the computer. The signal w

represents measurable disturbances to the model, namely, the fraction f_{N_2} of nitrogen in the current breathing gas as well as the blood perfusion ω_i to muscle and fat tissues, which can be estimated from heart-rate measurements [12].

Predictor

In the formulation of the optimal control problem we want to use model (2)–(8) to predict the output for a given decompression procedure defined through the input trajectory of u. Future expectations are required for the blood perfusion ω_i, which is assumed to have a fixed, expected value. If the diver has any expectations about the workload for the dive, then he or she can manipulate the predicted ω_i. The term f_{N_2} can change according to scheduled tank switches during the dive. A block diagram showing the structure of the optimal control problem in conjunction with the state observer is given in Figure 2.

As seen from (1), bubble growth $\dot{r}_i$ is positive for a negative input u, hence the output starts growing immediately upon ascending. However, in a typical dive, significant growth appears after reaching the surface, when positive supersaturation in the tissues $p_{t,1} - P_{\text{amb}}$ and $p_{t,2} - P_{\text{amb}}$ keeps $\dot{r}_i$ positive for a period of time. At some point the bubble volume reaches its peak and starts decaying again due to the oxygen window [22]. It is this peak we want to limit through the formulation of a constrained nonlinear optimization problem. For the input trajectory $\mathbf{U} = [u_0\, u_1 \cdots u_{n-1}]$ there exists an output trajectory $\mathbf{Y}(\mathbf{U}, x_k) = [y_1\, y_2 \cdots y_n]$ given by numerical integration of (2)–(8), where x_k is the current state from the observer and n is the number of integration steps over the predicted horizon. Consequently, the peak output is given by

$$y_{\text{peak}}(\mathbf{U}, x_k) = \max(\mathbf{Y}(\mathbf{U}, x_k)). \tag{11}$$

Optimal Control Formulation

A decompression procedure can be expressed in terms of the vector of stop times

$$\mathbf{t} = \begin{bmatrix} t_1 & t_2 & \cdots & t_m \end{bmatrix}, \tag{12}$$

where m is the number of stops and t_i is the stop time at the pre-defined design-variable stop depth ρ_i, which is a component of the stop vector

$$\rho = \begin{bmatrix} \rho_1 & \rho_2 & \cdots & \rho_m \end{bmatrix}, \tag{13}$$

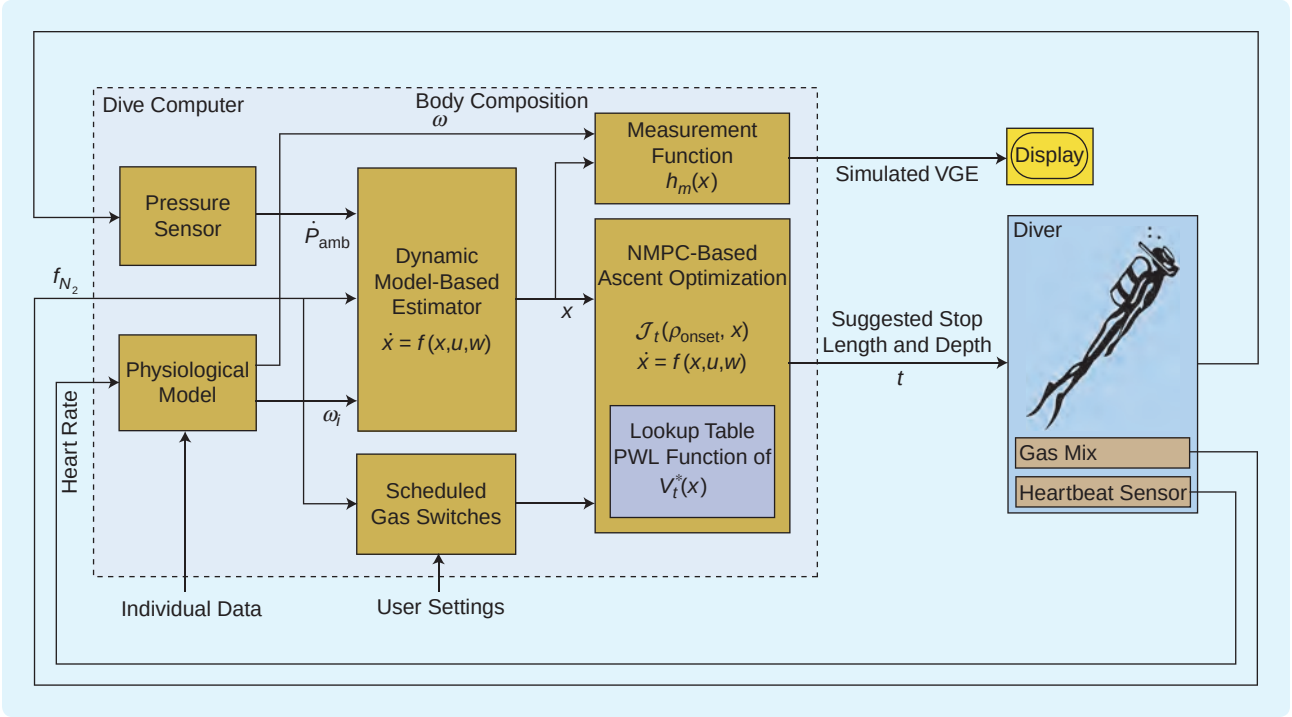

FIGURE 2 Dive-computer implementation. This diagram illustrates how the model equations (2)–(8) are used for the state estimator and model predictive control formulation. The pressure sensor provides the input u to the estimator, whereas the current selected gas mix f_{N_2} and tissue blood perfusion ω_i are treated as components of the model noise w. The signal ω_i is explicitly estimated from heart-rate measurements through the physiological model. The state vector x is the parameter vector of the optimization problem. The vector x is also provided to the measurement function $h_m(x,w)$, which is used to visualize bubble growth on the computer display for the diver. The suggested optimal stop schedule is interpreted by the diver, and the pressure measurement provides feedback for an updated model estimate.

where $\rho_i < \rho_{i+1}$. The stop depths are given in meters sea water (msw), which is a pressure unit for the equivalent depth in sea water. The pressure in water increases by approximately 10 kPa for each meter depending on temperature and salinity. Traditionally, intervals of 3 msw are chosen for decompression stops, but alternative stop regimes are used. For example, Revision 6 of the *U.S. Navy Diving Manual* [23] skips the shallowest stop at 3 msw, a practice also known from technical diving, where 100% oxygen is commonly used as the final decompression gas at 6 msw. The combination of $\mathbf{t}$ and ρ can explicitly describe the input trajectory $\mathbf{U}$ for the prediction horizon. Since we want the optimizer $\mathbf{t}$ to be continuous, the integration of (2)–(8) is done by keeping n constant and adjusting ΔT to achieve the desired horizon.

Decompression wastes time, costs money, and increases the risk of a dive by prolonging it and can thus be considered as a "necessary evil" for preventing DCS. Consequently, divers want to minimize the time spent under water decompressing. This amount of time is expressed by the cost function

$$J(\mathbf{t}) = \sum_{i=1}^{m} t_i. \tag{14}$$

Reparameterization of the Decompression

The vector $\mathbf{t}$ represents a staged decompression. According to the characteristics of the Copernicus model, the VGE peak $y_{\text{peak}}(\mathbf{U}, x_k)$ is often weakly associated with how the decompression time is distributed between the various stop depths [11]. The two quantities that dominate the outcome of a decompression are the total decompression time and how deep the schedule starts. Hence, it is advantageous to reparameterize the vector $\mathbf{t}$ to be described by these two quantities.

Additionally, an arbitrary shape generated by $\mathbf{t}$ is not wanted from a practical perspective. Divers prefer a predictable ascent scheme with as few surprises as possible. Traditionally, decompression schedules follow an exponentially decaying shape due to first-order gas-elimination dynamics. This practice is proven to provide safe decompression and is popular and convenient to follow by divers. Hence, we aim to design an exponential schedule parameterized by the total decompression time and onset depth, that is,

$$z = [t_{\text{total}}, \rho_{\text{onset}}], \tag{15}$$

where t_{total} is the total decompression time and ρ_{onset} is a continuous variable defining the decompression onset depth. Alternative shapes that yield smaller t_{total} are possible [19], however, we do not recommend such untested regimes since the data foundation is too weak to extrapolate the model domain. The linear ascent from the onset depth ρ_{onset} to t_{total} can be expressed as the accumulated decompression time

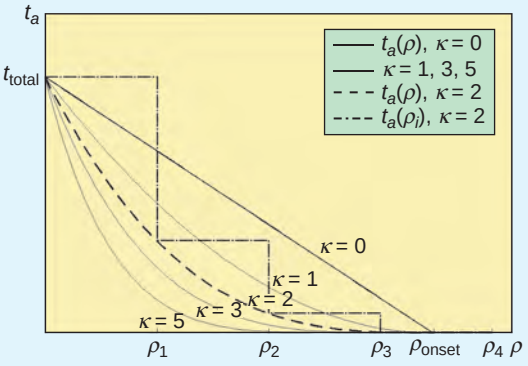

FIGURE 3 Two-variable representation of the decompression profile. The profile is explicitly defined by the parameters ρ_{onset} and t_{total}. Equation (16) is illustrated here for several values of κ. A stepwise procedure at the stop depths in ρ is shown for $\kappa = 2$. Note that time is on the vertical axis since accumulated decompression time t_a is a function of ρ_i.

$$t_{a,\text{lin}}(\rho) = a_p\rho + b_p, \tag{16}$$

where $a_p = -(t_{\text{total}}/\rho_{\text{onset}})$ and $b_p = t_{\text{total}}$. The desired shape is achieved by extending the parameterization with a polynomial function described by a curvature parameter κ, which gives

$$t_a(\rho) = \frac{1}{b_p^{\kappa}}(a_p\rho + b_p)^{k+1}. \tag{17}$$

The value $\kappa = 2$, which enforces a practically convenient decompression shape, is used in the examples below. Equation (16) is plotted for several values of κ in Figure 3, which illustrates how the accumulated decompression time is given for the discrete stop depth ρ_i. The individual stop times are then given by

$$t_i = t_a(\rho_{i-1}) - t_a(\rho_i), \tag{18}$$

where $\rho_0 = 0$. Expression (17) explicitly yields the vector $\mathbf{t}$ in (11), reparameterized by z, which can describe any decompression procedure for practical applications. To achieve the desired decompression procedure, a threshold for model-based bubble growth is added to the constraints. The resulting optimization problem is formulated as

$$V^* = \min_z J(\mathbf{t}(z)), \tag{19}$$

subject to

$$t_{\text{total}} \geq 0, \tag{20}$$

$$\rho_{\text{onset}} \geq 0, \tag{21}$$

$$y_{\text{peak}}(\mathbf{U}(z), x_k) \leq y_{\text{thresh}}, \tag{22}$$

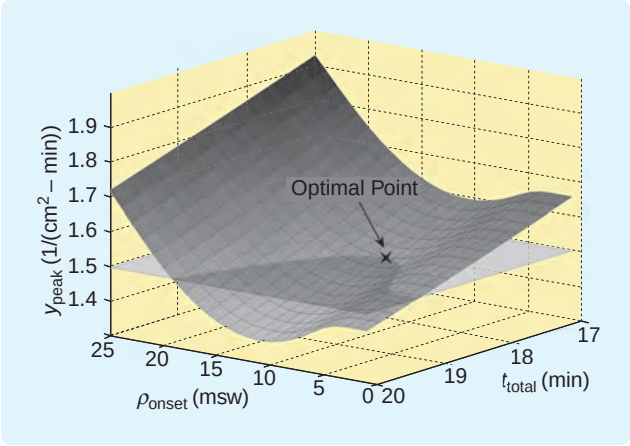

FIGURE 4 Optimization of decompression. The peak bubble score is plotted as a function of the decompression procedure. $y_{peak}(z)$ is calculated from a dive to 30-msw depth and 30-min bottom time for a range of decompression procedures described by the two-variable representation $z = [t_{total}, \rho_{onset}]$. The constraint level $y_{thresh} = 1.5$ is plotted as a transparent plane. The optimal point is at the bottom of the curve formed by the cross section between the function surface and the threshold plane.

where V^* is the optimal cost function, $y_{peak}(z, x_k)$ is obtained from (10) parameterized by z, and y_{thresh} is the peak value of VGE considered to be adequately safe. The problem (19)–(22) can be solved using a numerical optimization algorithm suitable for nonlinear constrained problems, where z^* denotes the optimal solution.

Example 1

All simulation examples use the model parameters given in [11], which are repeated in Table 1. To illustrate the characteristics of (19)–(22), a dive to 30-msw depth and 30-min bottom time is simulated to give the initial state x_k from (2)–(8). The constraint function (10) is then plotted in terms of z, as illustrated in Figure 4. A tolerable VGE peak $y_{thresh} = 1.5$ is plotted as a transparent plane. The optimal solution in this simulation example is found to be

$$z^* = \begin{bmatrix} t^*_{total} & \rho^*_{onset} \end{bmatrix} = \begin{bmatrix} 18.2 \text{ min} & 10.7 \text{ msw} \end{bmatrix}. \quad (23)$$

The time response of this optimal solution is plotted in Figure 5. z^* yields $\mathbf{t} = [11.3\ 5.23\ 1.49\ 0.08]$ for $\rho = [3\ 6\ 9\ 12]$, which gives the input trajectory $\mathbf{U}(z)$. The optimal depth profile is plotted together with the model-predicted output peak, which reaches the threshold $y_{thresh} = 1.5$.

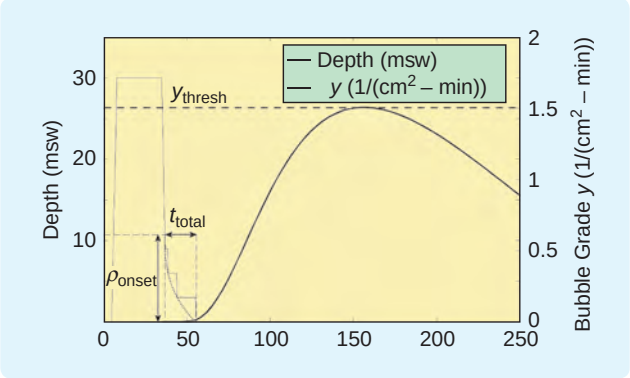

FIGURE 5 Simulated time response of bubble growth. The depth profile (left vertical axis) and y response (right vertical axis) following the optimal decompression calculated from the example in Figure 4.

TRANSFORMATION TO BOX-CONSTRAINED NONLINEAR OPTIMIZATION

To improve computational efficiency, (19)–(22) can be transformed to a simpler problem. The nonlinear constraint (21), which is always active for feasible decompression dives, yields

$$y_{peak}(t_{total}, \rho_{onset}, x_k) = y_{thresh}. \quad (24)$$

If there exists a decompression procedure, that is, a nonzero t_{total} for which the equality (23) holds, then the total decompression time can be given as a function of the onset depth ρ_{onset}, that is,

$$t_{total} = J_t(\rho_{onset}, x_k), \quad (25)$$

where J_t is a transformed cost function found by solving the nonlinear equation (24) with respect to t_{total}. The function J_t requires logic to handle cases where (24) is unsolvable, for instance, when the dive is too short to require decompression and y_{thresh} is not reached even with a free ascent. Now ρ_{onset} can be selected as the transformed optimizer, and the box-constrained nonlinear problem can be formalized as

$$V^*_t(x_k) = \min_{\rho_{onset}} J_t(\rho_{onset}, x_k), \quad (26)$$

subject to (20) and (21).

Problem (26) is computationally more efficient than (19)–(22) since the computationally demanding model predictor is moved from the constraints to the cost function, leaving only optimizer bounds as constraints. Such problems, which are classified as box constrained, can be solved with unconstrained optimization solvers, which are simpler than methods handling nonlinear constraints. The dimension of the optimizer is also reduced from 2 to 1. The original optimizer is computed by

$$z^* = [V^*_t(x_k) \quad \rho^*_{onset}]. \quad (27)$$

Computational efficiency can be further improved by using a barrier function for the model-predicted constraint

[19]. This approach avoids solving the nonlinear equation (23) and the logic handling.

Example 2

Example 1 is now used to demonstrate the transformed problem (25). The transformed cost function is plotted in Figure 6. The minimum of the curve yields the same solution as in Example 1.

SIMULATION RESULTS

Feedback from Heart-rate Measurement

The optimal control law in (25) is solved at each instant of time with updated information of u_k and w_k. This approach of calculating the input is called an MPC problem. To illustrate the effect of measurement feedback on MPC, we simulate a dive where the workload during decompression is higher than anticipated in the predictor. As a baseline we use the same 30-msw depth and 30-min bottom time as in Example 1, and the results are shown in Table 2. Without knowledge about future heart rate, the optimal control problem is solved with the predictor using a fixed heart rate of 95 beats per minute (b/min). However, the state estimator is continually updated with the current heart-rate measurement of 120 b/min to provide an updated state vector for the MPC problem throughout the decompression. The results illustrate how the elevated workload during decompression increases nitrogen washout, thereby allowing the predictor to try shorter stop times without violating the bubble-growth constraint. This lowered partial pressure gradually shortens the next decompression stop and, consequently, the total decompression time. However, after the first 12-msw stop, we see a slight increase from 18.2 min to 18.5 min total decompression time because the workload at 12 msw slightly increases nitrogen on-gassing at this depth. In total, this elevated workload reduces total decompression time from 18.2 min to 13.9 min.

Exposure Scaling

In [24] it is shown that if the combination of time and depth is too strenuous, then the risk of DCS increases regardless of the decompression model used. This study confirms the empirical observation that the risk of DCS depends on the type of exposure. In contrast, most decompression tables and computer algorithms are designed to satisfy a fixed level of risk. The Haldanian principle [3] sets a tolerable supersaturation ratio, which is refined by using M-values, gradient factors, free-gas volume, or other instantaneous stop criteria. From a theoretical perspective it is expected that the procedures from a given model keep the diver at a consistent level of risk regardless of exposure. The mentioned study indicates that this is not the case. The same point was emphasized as early as 1951 when it was stated that "… there are sharply demarcated limits of perhaps 5 ft in diving depth and several thousand feet in altitude ascent separating injury from a state of well-being" [25].

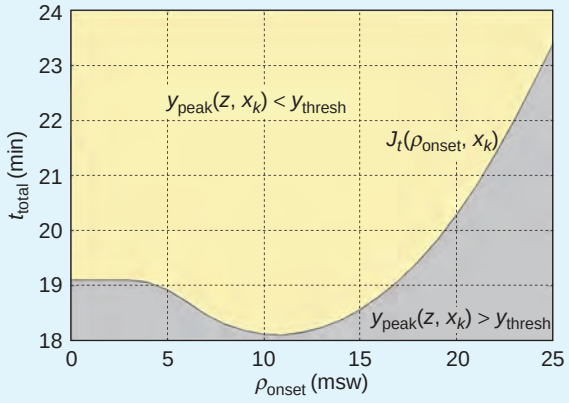

FIGURE 6 The transformed cost function. By forcing the inequality constraint (21) to be active and defining the equality constraint (23), the total decompression time t_{total} can be plotted as a function of ρ_{onset}, which is the new cost function $V_t(x_k,\rho_{onset})$. This dive is the same as in Example 1. The shaded area denotes where the inequality constraint is violated.

Evaluating how the required total decompression time scales with more strenuous exposures is a relevant benchmark for illustrating how various algorithms differ in practice for the diver. To maintain a consistent level of bubble formation and DCS risk, the decompression time required is expected to increase more rapidly for scaling exposures than traditional algorithms suggest. To demonstrate the effect of MPC on this issue, we compare the total decompression time of Copernicus with procedures from other algorithms, namely, RGBM, VPM-B, and Bühlmann. The procedures are calculated using V-Planner [26] and GAP [27] software using the configurations RGBM

TABLE 2 Results from Example 3. The optimal decompression schedule for a dive to 30-msw depth and 30-min bottom time is presented as the vector $t = [t_1\ t_2\ t_3\ t_4]$. The result is reoptimized at each depth after completion of the planned stop time, and a new vector is presented for the upcoming stop depths. The total decompression time t_{total} at each line is calculated as the sum of the previous stops and the remaining time after reoptimization. t_{total} gradually decreases due to elevated heart rate during decompression. Note that the initial solution at 12 msw is identical to the solution in Example 1.

Depth ρ_i [msw]	Reoptimized schedule t [min]	t_{total} [min]	t_i [min]
30	—	—	30
12	[11.312, 5.2195, 1.4841, 0.0784]	18.2	0.0784
9	[11.571, 5.3387, 1.5180, 0.0000]	18.5	1.5180
6	[10.933, 5.0430, 0.0000, 0.0000]	17.6	5.0430
3	[7.2336, 0.0000, 0.0000, 0.0000]	13.9	7.2336

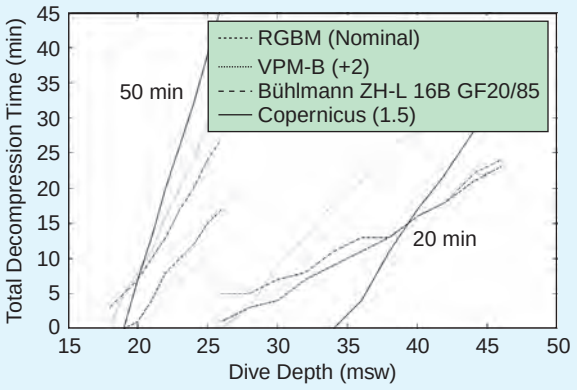

FIGURE 7 Exposure scaling for depth. This plot shows how the total decompression time increases with depth for two fixed bottom times, namely, 20 min and 50 min, within the selected models.

(nominal), VPM-B (+2), and Bühlmann (ZH-L16B GF20/85). We initiate the calculation on four exposures, where bottom time is fixed for two simulations and depth is fixed for the two remaining simulations, and where total decompression time is calculated for a range of depths and bottom times, respectively. For Copernicus, a consistent VGE peak threshold of $y_{\text{thresh}} = 1.5$ is used.

The results plotted in figures 7 and 8 show how total decompression time increases much faster in Copernicus for scaling exposures. In particular, long bottom times appear to be punished significantly by Copernicus. This result is coherent with the U.S. Navy's conclusions as stated in the preface of [23], where particularly long and shallow air exposures give an unacceptable high risk of DCS.

DISCUSSION

Decompression of divers is a complex process involving bubble formation, as described by nonlinear differential equations. There exists no analytical solution to limit bubble formation by using state feedback. Since bubble growth and DCS onset are delayed events following decompression, a feasible approach to designing optimal control laws is through an MPC formulation. A natural step forward in decompression modeling is to adopt tools from modeling and control applications.

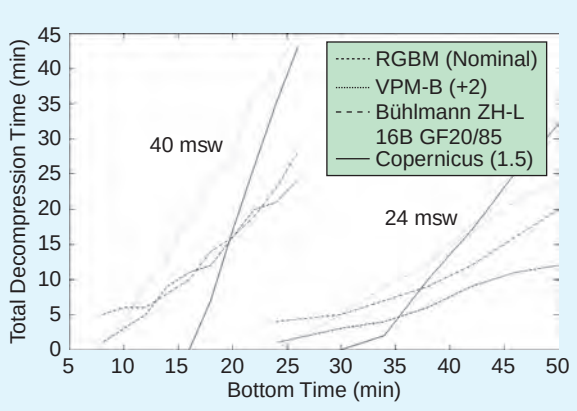

FIGURE 8 Exposure scaling for bottom time. This plot shows how the total decompression time increases with the bottom time for two fixed depths, namely, 24 msw and 40 msw, within the selected models.

Explicit MPC

While the purpose of this article is to present the basic concepts of optimal decompression procedures in the context of MPC, it is clear that certain aspects need careful consideration before the procedures can be robustly implemented in a typical dive-computer architecture constrained by low cost and a minimum number of clock cycles to ensure that battery endurance is as high as ten years. The use of explicit nonlinear MPC [28] is ideally suited for this purpose, where an approximate explicit state-feedback law in terms of a piecewise control law is precomputed and stored in a lookup table for efficient online computations. It has been demonstrated that optimal decompression procedures for dives down to 50 msw and up to 64 min can be implemented with online processing of only 20 fixed-point arithmetic operations per recalculation, typically every 4 s [20]. Using the approach in [29], a lookup table containing about 4600 quadratic control laws is precomputed to approximate the optimal solution, which means that the flash memory of the dive computer is the limiting computer resource. A different solution strategy for the optimal control problem is described in [19], where barrier functions are used to efficiently handle cases when no feasible solution exists or free ascent is feasible. Considering the high-volume consumer market for dive computers, it is possibly beneficial to design dedicated integrated circuits for the dive-procedure calculations, such as ASICs that can implement explicit nonlinear MPC control law computations using about 20,000 transistors [30], in addition to memory, or FPGAs that have similar complexity.

Measurement Sensors

The lack of measurable objective outputs entails challenges when developing modeling and control systems. Without an adequate model, it is difficult to define a control law with known properties. Despite its relevance for DCS being disputed, VGE is gaining more acceptance and is widely accepted in decompression research as the only objective measure of decompression stress.

Ultrasonic measurement of vascular bubble formation has a major weakness in that it cannot be measured during the dive or throughout the decompression. The techniques are also coarse and do not provide measurements of the expansion or compression of bubbles in the periphery, which is relevant during the dive. Since techniques are not

Decompression modeling of divers is a research field that is over 100 years old and since the beginning has been studied mainly as a clinical and biomedical problem.

available for measuring the state vector in real time, it is not possible to develop a state observer for bubble formation in a diver. The accuracy of the model's predictive control formulation is limited by the partial open-loop model estimate of bubble formation, with feedback only from ambient pressure and, possibly, heart beat.

Efforts are being made to develop techniques for measuring micro bubbles at an early stage, for example, dual-frequency ultrasound and optical instruments. However, these techniques are not close to being operational. If it were possible to measure the compression of bubble nuclei and the very first expansion during ascent, a more accurate feedback state observer, such as an extended Kalman filter, could be designed. Also the measurement of gas partial pressure in blood and tissue would improve observability of the system and provide feedback to the state observer. However, there is a similar lack of operational measurement techniques. A feedback observer would greatly improve the accuracy and consistency of risk reduction for decompressions calculated using MPC.

Practical Implications

Shifting the shape of the decompression procedure to shallower or deeper stops has been extensively tested experimentally, although with mixed results [31]–[34]. The concept of deep stops has received considerable interest during the last decades both among divers and in the scientific community. The idea was born when Richard Pyle discovered a personal benefit for his dives when he added deep stops on top of traditional procedures. This practice was picked up by the technical diving community and is now incorporated into various practices, which indicates that traditional procedures are sometimes inefficient. The formulation in this article considers optimal stops, and thus modifying the procedures by adding deep stops is not needed. Stopping shallower or deeper than the optimal depth schedule results in a suboptimal solution. If a more conservative procedure is desired, the schedule can be calculated with a lower y_{thresh}.

Another aspect demonstrated by results derived from Copernicus is how rapidly total decompression time increases with dive exposure. It appears to be a challenge to avoid violating the constraint of the optimization problem for longer and deeper dives. Making the assumption that the Copernicus model is valid, the formulation in this article defines a consistent stress level, which suggests that the decompression algorithms that are compared to Copernicus do not cope with longer and deeper dives in a satisfactory manner. The present results conclude that there is a need for the decompression time scale to be increased far more rapidly than anticipated.

CONCLUSIONS

Decompression modeling of divers is a research field that is over 100 years old and since the beginning has been studied mainly as a clinical and biomedical problem. The topic is largely unexplored by the technological sciences using methods and theories for modeling and control. This article outlines a structure where the process of bubble formation is modeled as a nonlinear dynamic model and then used to design a state estimator and model-based predictor. Procedures are then calculated using explicit MPC. We further discussed dive-computer implementations using approximate explicit solutions. Finally, we showed practical differences for divers using computers that implement this approach. When future advances in sensor technology are made, the present structure can be further developed to include more feedback control of the estimator and optimal control formulation.

ACKNOWLEDGMENTS

This work has been supported by UWATEC AG, Switzerland and by the Norwegian Petroleum Directorate, Norsk Hydro, Esso Norge and Statoil under the "dive contingency contract" (no. 4600002328) with Norwegian Underwater Intervention (NUI).

AUTHOR INFORMATION

Christian R. Gutvik received the Siv.Ing (M.Sc.) in control engineering from the Norwegian University of Science and Technology (NTNU) in 2003. He worked as a research fellow in the Department of Circulation and Medical Imaging at the medical faculty from 2003 to 2008, where he developed the Copernicus decompression model. He is currently a group manager for control systems in a private company. His interests include biomedical modeling and optimal control.

Tor A. Johansen received the Dr.Ing. (Ph.D.) in electrical and computer engineering from NTNU in 1994. From 1995 to 1997 he was a research engineer with SINTEF Electronics and Cybernetics. Since 1997 he has been a professor in engineering cybernetics at NTNU. He has been a research visitor at the University of Southern California,

the Technical University of Delft, and the University of California, San Diego. He was an associate editor of *Automatica* and *IEEE Transactions on Fuzzy Systems*. His research interests include optimization-based control and industrial application of advanced control. He has published more than 60 journal papers.

Alf O. Brubakk is a professor of environmental physiology at NTNU. He received the doctorate in medicine in 1978 and was one of the founders of the medical faculty in Trondheim. He has contributed to the understanding of how gas bubbles form and how they can injure the diver. He is an editor of the fifth edition of *The Physiology and Medicine of Diving*, and has published more than 100 journal papers. He has also worked on other aspects of environmental physiology, including the effects of cold and space environment.

REFERENCES

[1] W. P. Butler, "Caisson disease during the construction of the EADs and Brooklyn bridges: A review," *Undersea Hyperb. Med.*, vol. 31, no. 4, pp. 445–459, 2004.

[2] P. Tikuisis and W. A. Gerth, "Decompression theory," in *Bennet and Elliott's Physiology and Medicine of Diving*, 5th ed., A. O. Brubakk and T. S. Neuman, Eds. Philadelphia, PA: Saunders, 2003, ch. 10.1, pp. 419–454.

[3] A. E. Boycott, G. C. C. Damant, and J. S. Haldane, "The prevention of compressed-air illness," *J. Hyg.*, vol. 8, pp. 342–443, 1908.

[4] D. E. Yount and D. C. Hoffmann, "On the use of a bubble formation model to calculate diving tables," *Aviat. Space Environ. Med.*, vol. 57, pp. 149–156, 1986.

[5] B. R. Wienke, "Reduced gradient bubble model," *Int. J. Biomed. Comput.*, vol. 26, no. 4, pp. 237–256, Nov. 1990.

[6] P. Tikuisis, C. A. Ward, and R. D. Venter, "Bubble evolution in a stirred volume of liquid closed to mass transport," *J. Appl. Physiol.*, vol. 54, pp. 1–9, 1983.

[7] M. L. Gernhardt. (1991). Development and evaluation of a decompression stress index based on tissue bubble dynamics. Ph.D. dissertation, Univ. Pennsylvania [Online]. Available: http://repository.upenn.edu/dissertations/AAI9211935/

[8] N. M. Gürmen, "Simulation of dynamic bubble spectra in tissues," *IEEE Trans. Biomed. Eng.*, vol. 48, no. 2, pp. 185–193, Feb. 2001.

[9] R. S. Srinivasan, W. A. Gerth, and M. R. Powell, "Mathematical model of diffusion-limited evolution of multiple gas bubbles in tissue," *Ann. Biomed. Eng.*, vol. 31, no. 4, pp. 471–481, 2003.

[10] C. R. Gutvik and A. O. Brubakk, "Copernicus—A dynamic 2-phase model for vascular bubble formation during decompression of divers," *IEEE Trans. Biomed. Eng.*, vol. 55, no. 3, pp. 884–889, 2009.

[11] C. R. Gutvik, R. G. Dunford, Z. Dujic, and A. O. Brubakk, "Parameter estimation of the copernicus decompression model with venous gas emboli in human divers," *Med. Biol. Eng. Comput.*, vol. 48, no. 7, pp. 625–636, 2010.

[12] C. R. Gutvik, U. Wisløff, and A. O. Brubakk, "Use of heart rate monitoring for an individualized and time-variant decompression model," *Eur. J. Appl. Physiol.*, vol. 110, pp. 885–892, 2010.

[13] J. Conkin, M. R. Powell, P. P. Foster, and J. M. Waligora, "Information about venous gas emboli improves prediction of hypobaric decompression sickness," *Aviat. Space Environ. Med.*, vol. 69, no. 1, pp. 8–16, 1998.

[14] O. S. Eftedal, H. Tjelmeland, and A. O. Brubakk, "Validation of decompression procedures based on detection of venous gas bubbles: A bayesian approach," *Aviat. Space Environ. Med.*, vol. 78, no. 2, pp. 94–99, Feb. 2007.

[15] D. Q. Mayne, J. B. Rawlings, C. V. Rao, and P. O. M. Scokaert, "Constrained model predictive control: Stability and optimality," *Automatica*, vol. 36, no. 6, pp. 789–814, June 2000.

[16] F. Doyle, L. Jovanovic, D. Seborg, R. S. Parker, B. W. Bequette, A. M. Jeffrey, X. Xia, I. K. Craig, and T. McAvoy, "A tutorial on biomedical process control," *J. Process Control*, vol. 17, no. 7, pp. 571–572, 2007.

[17] H. Lee, B. Buckingham, D. Wilson, and B. Bequette, "Closed-loop artificial pancreas using model predictive control and a sliding meal size estimator," *J. Diabetes Sci. Technol.*, vol. 3, no. 5, pp. 1082–1090, 2009.

[18] S. Galán and P. I. Barton, "Dynamic optimization of hybrid systems," *Comput. Chem. Eng.*, vol. 22, pp. 183–90, 1998.

[19] L. Feng, C. R. Gutvik, T. A. Johansen, and D. Sui, "Barrier function nonlinear optimization for optimal decompression of divers," in *Proc. IEEE Conf. Decision and Control*, Shanghai, 2009, pp. 1800–1805.

[20] L. Feng, C. R. Gutvik, and T. A. Johansen, "Optimal decompression through multi-parametric nonlinear programming," in *Proc. NOLCOS 8th IFAC Symp.* Abstracts, Bologna, Italy, 2010, pp. 56–57.

[21] O. Eftedal and A. O. Brubakk, "A method for detecting intravascular gas bubbles using 2D ultrasonic scanning and computer-based image processing," in *Proc. XVII Annu. Meeting EUBS*, E. Michalodimitrakis, Ed. Heraklion, Crete: EUBS, 1991, pp. 311–316.

[22] H. D. V. Liew, J. Conkin, and M. E. Burkard, "The oxygen window and decompression bubbles: Estimates and significance," *Aviat. Space Environ. Med.*, vol. 64, no. 9, p. 85965, 1993.

[23] N. S. S. Command, *U.S. Navy Diving Manual*, 6th ed. AquaPress, 2008.

[24] T. G. Shields, P. M. Duff, S. Wilcock, and R. Giles, "Decompression sickness from commercial offshore air-diving operations on the UK continental shelf during 1982 to 1988," in *Advances in Underwater Technology and Offshore Engineering*, vol. 23. Aberdeen, U.K.: The Society for Underwater Technology, Nov. 1989.

[25] A. B. Behnke, "Decompression sickness following exposure to high pressures," in *Decompression Sickness*, J. H. Fulton, Ed. Philadelphia, PA: Saunders, 1951, pp. 53–114.

[26] R. Hemingway and E. C. Baker. (2010). V-Planner, v3.81 [Online]. Available: http://www.v-planner.com

[27] K. Hofwegen and P. Fjelsten. (2009). GAP-software, v2.3 [Online]. Available: http://www.gap-software.com

[28] T. A. Johansen, "Approximate explicit receding horizon control of constrained nonlinear systems," *Automatica*, vol. 40, no. 2, pp. 293–300, Feb. 2004.

[29] A. Grancharova, T. A. Johansen, and P. Tøndel, "Computational aspects of approximate explicit nonlinear model predictive control," in *Assessment and Future Directions of Nonlinear Model Predictive Control*, L. Biegler, F. Allgöwer, and R. Findeisen, Eds. New York: Springer-Verlag, 2007.

[30] T. A. Johansen, W. Jackson, R. Schreiber, and P. Tøndel, "Hardware synthesis of explicit model predictive controllers," *IEEE Trans. Contr. Syst. Technol.*, vol. 15, no. 1, pp. 191–197, 2007.

[31] A. Marroni, P. B. Bennett, F. J. Cronje, R. Cali-Corleo, P. Germonpre, M. Pieri, C. Bonuccelli, and C. Balestra, "A deep stop during decompression from 82 fsw (25 m) significantly reduces bubbles and fast tissue gas tensions," *Undersea Hyperb. Med.*, vol. 31, no. 2, pp. 233–243, 2004.

[32] N. A. Schellart, J. J. Corstius, P. Germonpré, and W. Sterk, "Bubble formation after a 20-m dive: Deep-stop vs. shallow-stop decompression profiles," *Aviat. Space Environ. Med.*, vol. 79, no. 5, pp. 488–494, 2008.

[33] C. R. Gutvik, A. Møllerløkken, and A. O. Brubakk, "Difference in bubble formation using deep stops is dependent on length of bottom time—Experimental findings and theoretical support," in *Proc. 33rd Annu. Scientific Meeting of the EUBS*. Sharm El Sheikh: European Underwater and Baromedical Society, 2007, pp. 146–149.

[34] W. A. Gerth, K. A. Gault, and D. J. Doolette, "Empirical evaluation of the efficacy of deep stops in air decompression dives," *Undersea Hyperb. Med.*, vol. 34, no. 4, pp. 231–232, 2007.

[35] T. Langø, T. Mørland, and A. O. Brubakk, "Diffusion coefficients and solubility coefficients for gases in biological fluids and tissues: A review," *Undersea Hyperb. Med.*, vol. 23, no. 4, pp. 247–272, 1996.

[36] W. D. McArdle, F. I. Katch, and V. L. Katch, *Essentials of Exercise Physiology*, 2nd ed. Philadelphia: Lippincott Williams and Wilkins, 2000.